Geochemical Perspectives Letters

Titanium isotope constraints on the mafic sources and geodynamic origins of Archean crust

L. Hoare, L.J.A. Rzehak, S. Kommescher, M. Jansen, M.T. Rosing, T. Nagel, M.-A. Millet, J. Elis Hoffmann, R.O.C. Fonseca

Supplementary Information

The Supplementary Information includes:

- 1. Samples
- 2. Methods
- 3. Thermodynamic Phase Equilibria Modelling
- 4. Trace Element Modelling
- 5. Modelling of Ti Isotope Fractionation
- Tables S-1 to S-11 (Tables S-2 to S-11 are available from the online version of this article at https://doi.org/10.7185/geochemlet.2342).
- Figures S-1 to S-4
- Supplementary Information References

1. Samples

All samples measured in this study have previously been characterised for their petrography, major and trace element compositions, and, in some instances radiogenic isotopes. Detailed geologic context, petrography, analytical methods, and major and trace element compositions of all tonalite and intracrustal differentiates can be found in Hoffmann *et al.* (2011a, b, 2014). The same information for all Isua tholeiitic metabasalt samples is sourced from Polat and Hofmann, 2003; Hoffmann *et al.*, 2011b. All geochemical data used in this study can be found in Tables S-3 to S-5 and S-9 to S-11. A brief outline of the sample petrography and major element geochemistry is provided below.

The mafic rocks analysed in this study consist of amphibolite facies tholeiitic to picritic metabasalts and metagabbros from the 3800 Ma (previously called the outer arc domain by Jenner *et al.*, 2009) and 3700 Ma (referred to as the inner arc domain by Polat and Hofmann 2003) terranes within the Isua Supracrustal Belt (ISB) in southwest Greenland. The ISB mafic rocks exhibit low SiO_2 (45.9–54.5 wt. %), low TiO_2 (0.6–1.1 wt. %), low to moderate Al_2O_3 (7.9–14.2 wt. %), low to moderate Na_2O (0.3–3.7 wt. %), moderate to very high MgO (5.2–20.1 wt. %), low K_2O (0.01–1.40 wt. %) and Mg# from 46.1 to 75.4 (Table S-4). Igneous textures and minerals in these samples are not pre-served on the microscopic scale, and major mineral phases present include amphibole (hornblende, anthophyllite), plagioclase, chlorite, epidote, quartz, calcite, and titanite (*e.g.*, Polat and Hofmann 2003; Hoffmann *et al.* 2011a, b).

All Itsaq Gneiss Complex (IGC) TTGs analysed in this study were collected in the Isukasia terrane in the southwest portion of the Isua Supracrustal Belt (ISB). The samples possess ages that range between 3650 to 3890 Ma (*e.g.*, Næraa *et al.*, 2012). Most IGC meta tonalite and trondhjemite samples in our study are well preserved and exhibit magmatic textures (*e.g.*, Nutman *et al.*, 1999; Hoffmann *et al.*, 2014). The main mineral assemblages of these rocks comprise plagioclase, quartz, amphibole, and biotite with minor titanite, apatite and accessory Fe-Ti oxides. The IGC meta tonalites and diorites exhibit moderate to high SiO_2 (62.0–72.9 wt. %), low TiO_2 (0.2–0.8 wt. %), high Al_2O_3 (14.8–18.1 wt. %), high Na_2O (4.0–5.9 wt. %), low to moderate MgO (0.5–3.2 wt. %), low to moderate K_2O (0.9–2.5 wt. %) and Mg# from 31.9 to 49.5 (Table S-5).

2. Methods

2.1. Chemical separation of Ti

For the duration of this study sample preparation first requires digestion of 20–60 mg (amount is dependent on the TiO_2 concentration of the sample to achieve at least 5 µg of natural Ti) of fine-powdered silicate rock sample or geo-standard in concentrated 1:1 mixture of HNO_3 and HF at 130 °C for 72 hours. An additional 2 ml of concentrated HNO_3 is then added and evaporated to incipient dryness. Following this step, each sample is taken up in 500 µl of concentrated HNO_3 and dried down, this step is repeated 3 times. The sample is then taken up in 6 M HCl with the addition of ~40 mg of H_3BO_3 into the solution to ensure the removal of any fluorides that would sequester Ti out of the sample solution. Finally, an aliquot containing 5 µg of Ti is taken from the sample solution and mixed with a ^{47}Ti-^{49}Ti double spike in a 48:52 ratio based on the calibration of Kommescher *et al.* (2020) and taken up in 5 mL 12 M HNO_3 prior to column chemistry.

Titanium is separated from the sample matrix using Eichrom N, N, N, N' tetra-n-octyldiglycolamide (DGA) resin. The procedure adopted in this study is based on the method initially developed by Zhang *et al.* (2011) and later modified by Hoare *et al.* (2020) and Millet *et al.* (2016). The method is outlined in Table S-1. This study used a double pass chemistry. Following purification, Ti fractions are treated with a 1:1 mixture of concentrated HNO_3 and 30 % H_2O_2 to remove any organic material.

Table S-1 Summary of ion exchange chromatography procedure for Ti purification of samples for MC- ICP-MS analysis

Step	Acid	Volume (mL)
Cleaning	Milli-Q	20
	3M HNO_3	10
Conditioning	12M HNO_3	10
Introduction	Sample in 12M HNO_3	5
Wash	12M HNO_3	20
Collect Ti	12M HNO_3 + 1 wt. % H_2O_2	10
Cleaning	Milli-Q	20
	3M HNO_3	10

2.2. Ti double spike MC-ICP-MS measurements and data reduction

Titanium isotope composition measurements of reference solutions OL-Ti and Col-Ti were carried out using a Nu Plasma II MC-ICP-MS at the Cardiff Earth Laboratory for Trace Element and Isotope Chemistry (CELTIC), School of Earth and Environmental Sciences, Cardiff University to check the double spike calibration. Samples and geo-reference materials were measured using either a Thermo Fischer Neptune XT MC-ICP-MS at the Deutsches Bergbau Museum, Bochum or a Thermo Fischer Neoma MC-ICP-MS at Freie Universität Berlin. For measurements on the Nu Plasma II samples were introduced via an Cetac Aridus II desolvating nebuliser (flushed with Ar), whereas in for sessions using a Themo Fischer Scientific Neptune and Neoma an ESI Apex Omega was used (flushed with Ar and N_2).

Prior to measurements purified samples were diluted to concentrations of 250 ng/g (Neptune XT and Neoma) or 1000 ng/g (Nu Plasma II) of Ti Samples were taken up in 0.3 M HNO_3 + 0.005 M HF solution. All instruments were fitted with nickel (Ni) jet-sampler and Ni (H) skimmer cones. The measurements were performed in medium resolution mode, with a resolution power (5-95 % peak definition, ΔM/M) in the range of ~ 5,000 or up to ~ 8,000 when using the Thermo Fischer Neoma MC-ICP-MS. Such resolution was sufficient to clearly identify the peak shoulders of the Ti isotopes, and simultaneously to counter the effect of non-resolvable polyatomic interferences such as $^{28}Si^{19}F$ and $^{14}N^{16}O_2H^+$ that can be introduced via the analyte solution (0.3 M HNO_3 – 0.005 M HF), which give inference on ^{47}Ti. The 'peak shoulder' is used to define an interference-free mass range on the respective mass, as polyatomic interferences are typically heavier than the respective mass. Titanium ion beam intensity ranged from 20-60 V on amplifiers with 10^{11} Ω resistors in their feedback loop. Ca interference on ^{46}Ti and ^{48}Ti was monitored at mass 44 and corrected during data reduction if necessary. Measurements of an individual sample consisted of 60-80 cycles with an integration time of 8 s. To account for small unresolved polyatomic interferences on ^{47}Ti due to the presence of F from the sample solution and Si from the torch ($^{28}Si^{19}F$), samples are bracketed by measurements of the double spiked OL-Ti standard solution.

The compositions of Ti reference solutions (OL-Ti and Col-Ti) and geo-reference materials (JB-2, BCR-2, AGV-1, G2) are in good agreement with previous published values (see Tables S-1 and S-2). The $\delta^{49/47}Ti$ value for AGV-1 reported here is heavier than the bulk of previously reported values but is within error of the recently published value of Storck *et al.* (2023; Table S-2) which could suggest this geo-reference standard is homogenous for Ti isotopes. Additionally, $\delta^{49/47}Ti$ values presented here for JA-2 and JG-2 differ from the values obtained by He *et al.* (2020; Table S-2). Given the lack of data for these two standards it is currently unclear if these offsets are the result of sample heterogeneity or inter laboratory bias. Further digestions and measurements of these geo reference materials will be required to confirm this. It should be noted that the samples ran on Neptune XT MC-ICP-MS at the Deutsches Bergbau Museum possess slightly larger 95 % c.i. values as during this session samples were analysed for fewer cycles (60 as opposed to 80). The 2σ internal precision of our $\delta^{49/47}Ti$ measurements, expressed as 95 % c.i. ssb (confidence interval; standard-sample-bracketing) is generally within ±0.020 - 0.030 ‰. The geo-reference materials and Ti reference solutions measured over the course of this study yield a pooled 2s intermediate precision of ±0.025 ‰, which we take as the best estimate of the uncertainty of our measurements. Total procedural blanks were always below 20 ng Ti, thus contributing less than 0.1% to the total processed sample Ti and are therefore negligible.

Table S-2 Summary of Ti isotope compositions of Ti reference solutions and geologic reference materials.

Reference solution/Geo-reference material	δ^{49}Ti (‰)	95 % c.i.	2 s.d.	n
OL-Ti	-0.010	0.004	0.025	32
Col-Ti	0.184	0.006	0.034	19
FUB-Ti (AA-Ti solution)	-0.162	0.006	0.034	12
BCR-2	-0.013	0.010	0.008	4
JB-2	-0.038	0.012	0.029	4
G-2	0.477	0.013	0.025	3
JA-2	0.137	0.020	-	1
AGV-2	0.134	0.018	-	1
JG-2	1.045	0.020	-	1

Table S-3 Summary of Ti isotope compositions of measured samples.

Sample	Rock type	δ^{49}Ti (‰)	95 % c.i.	2 s.d.	n
2000-10	Metabasalt	0.078	0.017	0.038	2
2000-13	Metabasalt	0.020	0.012	-	1
2000-4	Metabasalt	0.024	0.020	-	1
2000-6	Metabasalt	0.006	0.026	-	1
2000-7	Metabasalt	0.031	0.027	-	1
2000-8	Metabasalt	0.046	0.042	-	1
jeh-2007-11	Metabasalt	0.079	0.019	-	1
2007-01	Metagabbro	0.049	0.015	0.030	2
2007-08	Pillow basalt	0.040	0.016	0.013	2
2007-14	Sheeted dyke	0.084	0.018	0.016	2
2007-15	Sheeted dyke	0.051	0.017	0.040	2
229467	Pegmatitic white gneiss	1.105	0.020	-	1
498033	Augen gneiss	0.527	0.020	-	1
jeh-SG-07	migmatitic tonalite	0.246	0.018	-	1
498027	migmatitic tonalite	0.782	0.020	-	1
498028	migmatitic tonalite	0.382	0.019	-	1
229403	metadiorite	0.230	0.020	-	1
496430	non-gneissic tonalite	0.325	0.020	-	1
SG09	non-gneissic tonalite	0.444	0.016	0.040	2
499337	non-gneissic tonalite	0.294	0.020	-	1

496431	non-gneissic tonalite	0.417	0.022	-	1
SG10	non-gneissic tonalite	0.453	0.019	-	1
jeh-SG-01	non-gneissic tonalite	0.878	0.019	-	1
SG04	non-gneissic tonalite	0.377	0.021	-	1
SG05	non-gneissic tonalite	0.189	0.018	0.066	2
JEH-2007-05	non-gneissic tonalite	0.386	0.019	0.047	2
JEH 10–18	non-gneissic tonalite	0.361	0.017	0.054	2
JEH 10–19	non-gneissic tonalite	0.419	0.022	-	1
JEH 10–25	non-gneissic tonalite	0.352	0.019	-	1
JEH 10–38	non-gneissic tonalite	0.287	0.019	0.027	2
JEH 10–39	non-gneissic tonalite	0.273	0.020	0.070	2

3. Theriak-Domino Thermodynamic Phase Equilibria Modelling

To assess the extent of elemental and Ti isotope fractionation during partial melting of metabasalts and crystallisation of tonalitic melts we employ the use of constraints from the latest generation of phase equilibria modelling. The modelling uses the Theriak algorithm (de Capitani and Brown, 1987). which is implemented via the Domino software (de Capitani and Petrakakis, 2010). The current version of the Domino software used in this study is distributed on GitHub and can be accessed using the following link https://github.com/Theriak-Domino/theriak-domino/. The complete output from the models including run conditions, the compositions and proportions of phases can be found in Table S-6. The procedure for thermodynamic modelling adopted in this study closely follows that of Nagel *et al*. (2012) and Hoffmann *et al*. (2014).

The references for the databases and solution models for all phases are outlined below:

Database: Holland and Powell (2011)

Solution models:
Amphibole - Green *et al.* (2016)
Melt, ilmenite, rutile, clinopyroxene, orthopyroxene and garnet - Holland *et al.* (2018)
Plagioclase - Holland *et al.* (2022)
Mica - White *et al.* (2014)

Set up for Theriak-Domino: Jørgensen *et al.* (2019)

These data are combined with relevant mineral-melt trace element partition coefficients (Table S-7) and Ti isotope fractionation factors (Table S-8). This will quantitatively test if these processes are viable mechanisms to explain the range of elemental and $\delta^{49/47}$Ti compositions observed in ISB metabasalts and IGC tonalites.

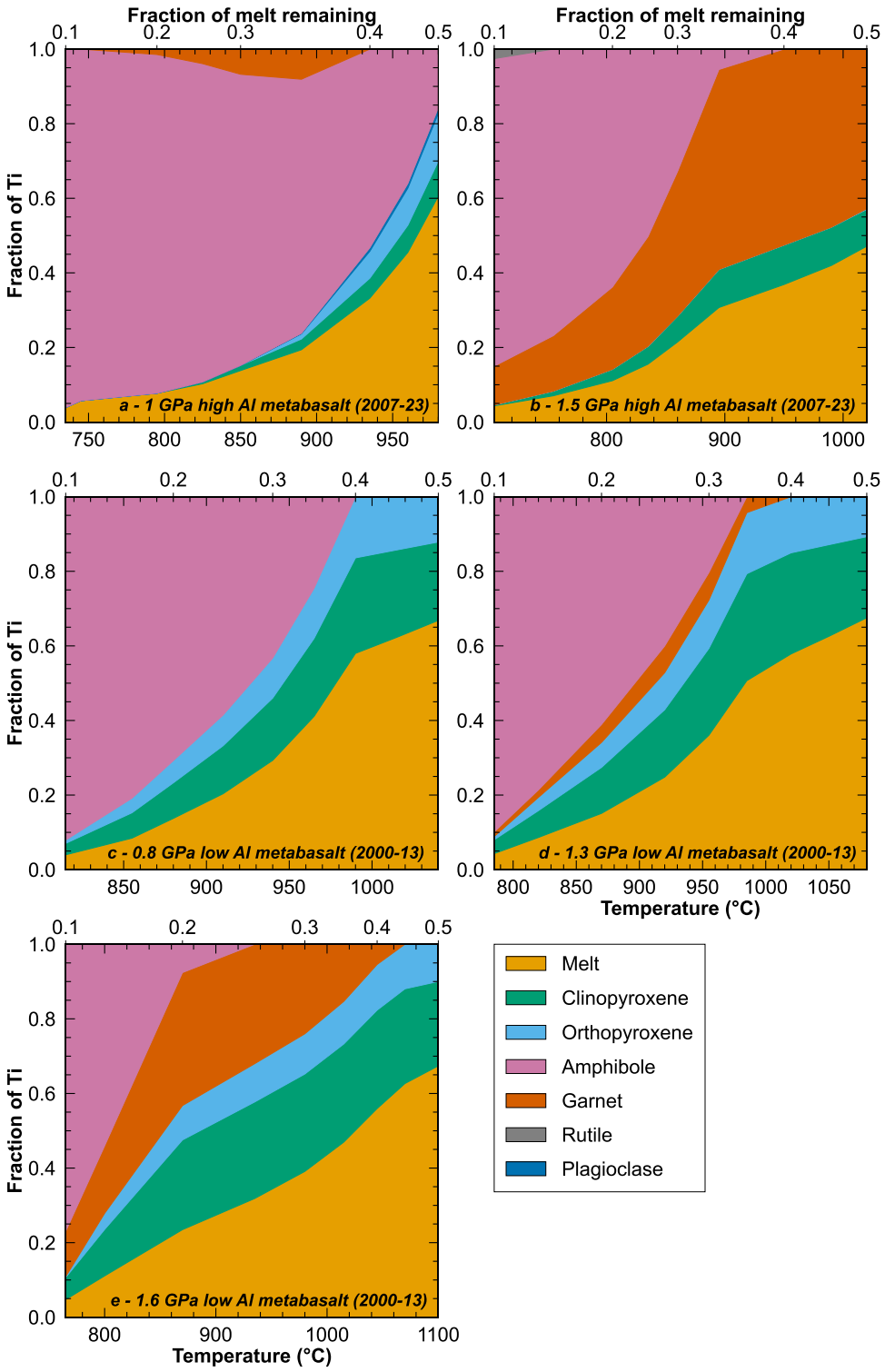

Figure S-1 Changes in the Titanium (Ti) budget of phases with respect to temperature and remaining melt fraction for partial melting of high-Al metabasalt sample 2007-23 at 1 GPa **(a);** and 1.5 GPa **(b)** and; low-Al metabasalt sample 2000-13 at 0.8 GPa **(c);** 1.3 GPa **(d);** and 1.6 GPa **(e)**.

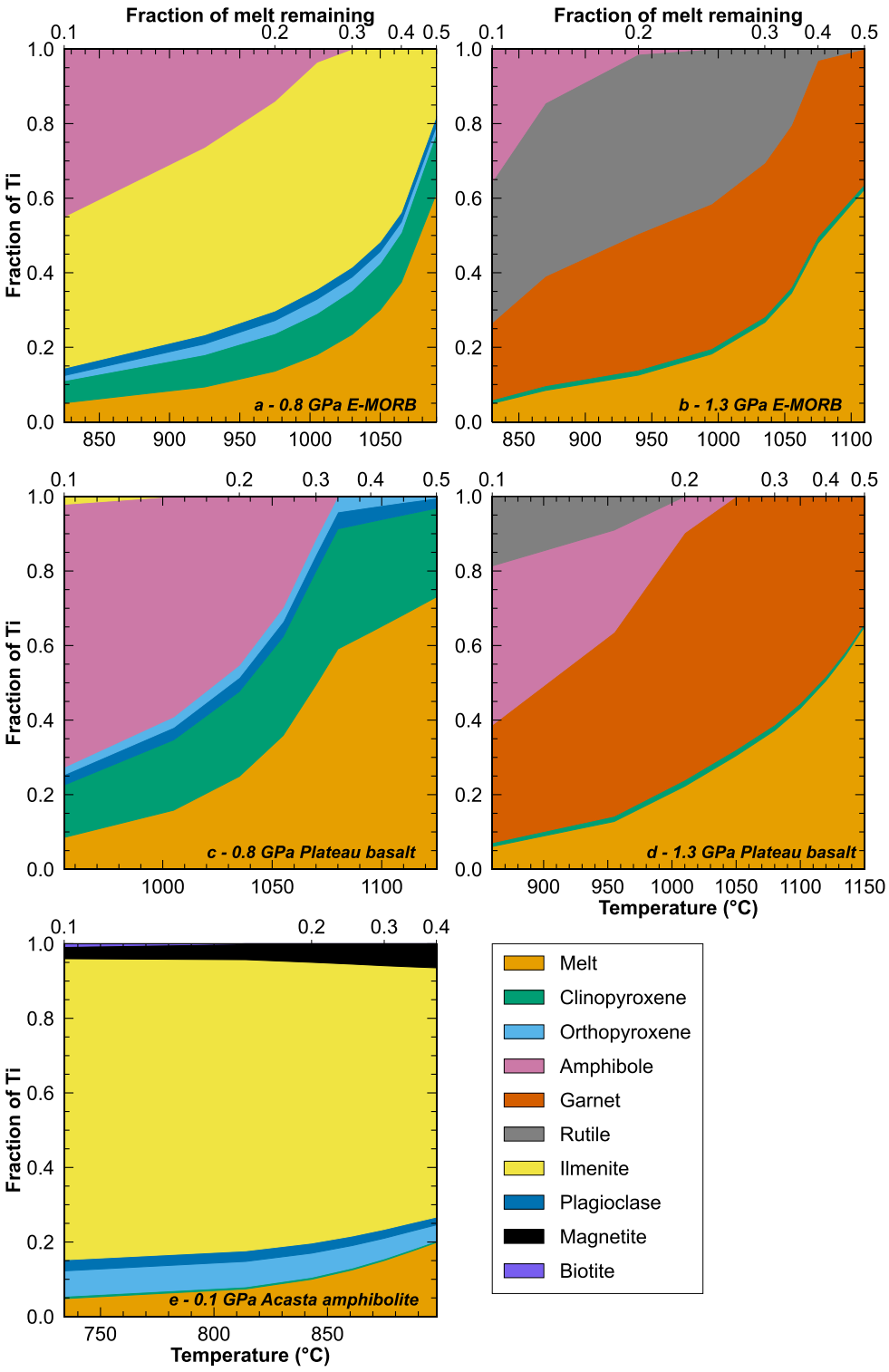

Figure S-2 Changes in the Titanium (Ti) budget of phases with respect to temperature and remaining melt fraction for partial melting of E-MORB (Gale *et al*., 2013) at 0.8 GPa **(a)** and 1.3 GPa **(b);** and a primitive flood basalt (Baffin island picrite; Kent *et al*., 2004) at 0.8 GPa **(c)** and 1.3 GPa **(d)**; and **(e)** an average Acasta amphibolite from (Johnson *et al*., 2018).

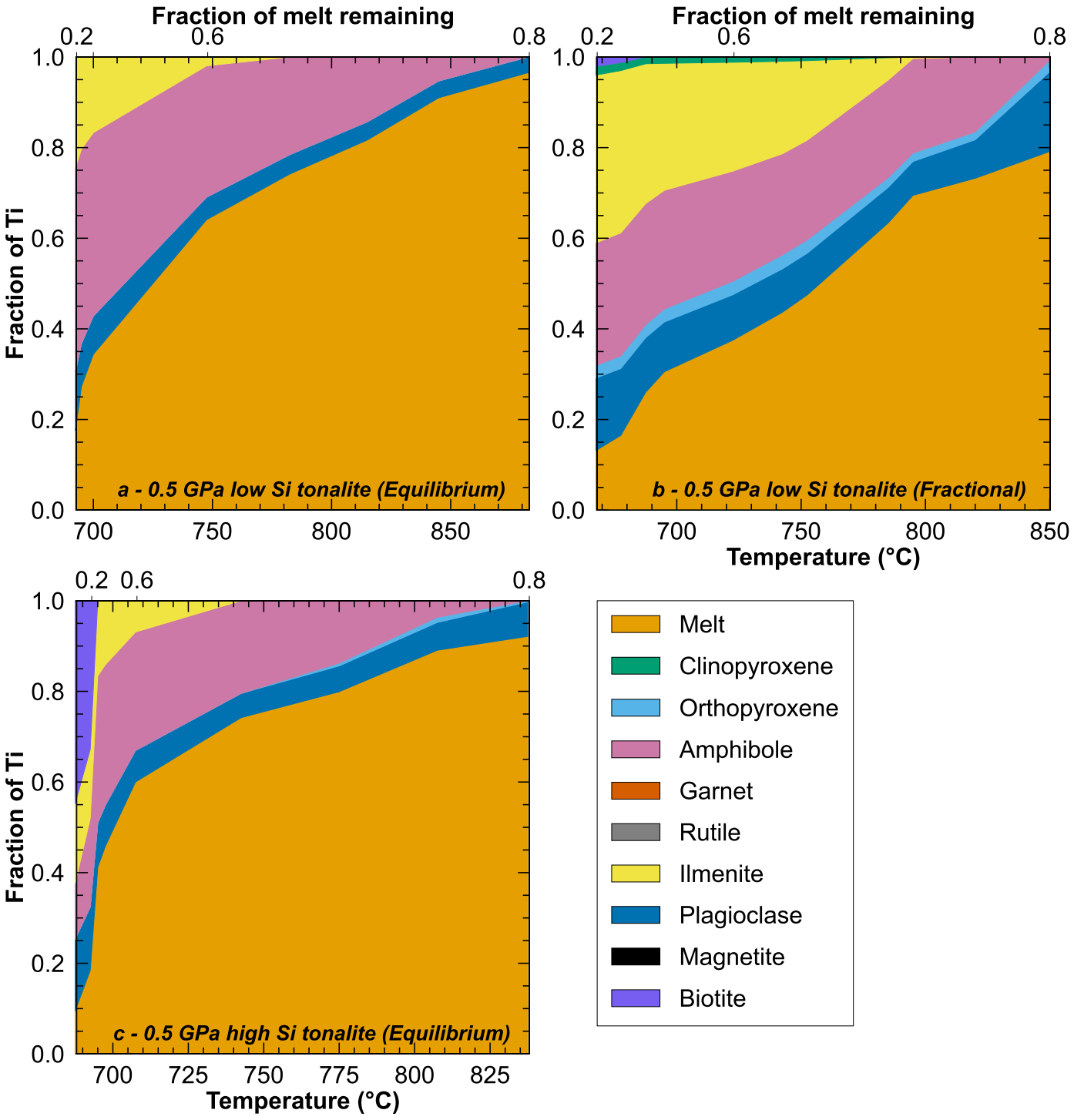

Figure S-3 Changes in the Titanium (Ti) budget of phases with respect to temperature and remaining melt fraction for equilibrium **(a)** and fractional **(b)** crystallisation of low-Si IGC tonalite sample G 97/31 at 0.5 GPa; and equilibrium crystallisation of IGC high-Si tonalite sample JEH 10-38 at 0.5 GPa **(c).**

Phase equilibria modelling is based on three scenarios using different mafic source compositions (see Table S-6, S-9, S-10). Firstly, hydrous partial melting of two metabasalts (high and low Al) representative of average compositions of local Eoarchean Isua mafic rocks (2007-23 - Hoffmann *et al.*, 2011b; 2000-13 - Polat and Hofmann, 2003), and then dehydration partial melting of E-MORB (Gale *et al.*, 2013), a picritic plateau basalt (Kent *et al.*, 2004), and an average amphibolite composition from the Acasta Gneiss complex (Johnson *et al.*, 2018). The initial H_2O contents used for the staring compositions was 4 wt. % and for Isua metabasalts, and 2 wt. % E-MORB and plateau basalt. The whole rock geochemistry of the starting compositions be found in Table S-6. Secondly, equilibrium and fractional crystallisation of two tonalite compositions (JEH 10-38 - Hoffmann *et al.*, 2011a; G97/31 - Nutman *et al.*, 1999). Amphibole is the dominant Ti-bearing mineral phase during partial melting of tholeiitic metabasalts (Fig. S-1, Tables S-6 and S-9), whereas depending on pressure, either ilmenite or rutile dominates during partial melting of E-MORB (Fig. S-2). Minor amounts Fe-Ti oxides only appear at low melt fraction (<10 %, Tables S-6 and S-9) for tholeiitic metabasalts (Table S-1 to 6). The distribution of Ti for low pressure (0.8 GPa) melting of a picritic plateau basalt is comparable to that of both tholeiitic metabasalts, except for minor amounts of ilmenite below 1000 °C, whereas at 1.3 GPa and below 1000 °C rutile hosts a significant portion of Ti (Figs. S-1, S-2). In stark contrast to the other partial melting models, ilmenite is the dominant Ti-bearing phase throughout the 0.1 GPa Acasta amphibolite model (Fig. S-2e, Table S-6, S-9). The appearance of amphibole and/or ilmenite causes the fraction of Ti hosted in the melt to sharply decline with decreasing melt fraction (Figs. S-1-3). Partial melting of the low-Al metabasalt produces plagioclase-free residues with clino- and orthopyroxene as the initially volumetrically dominant phases, until the appearance of amphibole below 1000 °C (Fig. S-1, Tables S-6 and S-9). Additionally, garnet is stabilised at ~ 1000 °C and 1050 °C at 1.3 and 1.6 GPa respectively in the low-Al metabasalt (Fig. S-1, Tables S-6, S-9) and at ~ 1100 °C for the high-Al metabasalt at 1.5 GPa (Fig. S-1, Table S-6, S-9). In the higher-pressure melting models garnet hosts a significant portion of Ti in the absence of amphibole or Fe-Ti oxides (Fig. S-1, S-2). Partial melting of high-Al metabasalt at 1 GPa produces plagioclase and notably less clinopyroxene compared to low-Al metabasalt (Fig. S-1, Tables S-6, S-9). Silicate melt is volumetrically dominant in the tonalite equilibrium and fractional crystallisation models, followed by plagioclase (Fig. S-3, Tables S-6, S-10). In the equilibrium models, amphibole, and biotite, along with minor amounts of ilmenite, quartz, and ortho- and clinopyroxene appear at lower temperature and melt fraction (Fig. S-3, Table S-6, S-10). In equilibrium crystallisation models, amphibole dominates the Ti budget of solid phases until the appearance of ilmenite, with biotite also sequestering a significant fraction of Ti at ~ 695 °C (Fig. S-3, Tables S-6, S-10). An abrupt transition occurs towards the latter stages of crystallisation (~ 80%) due to the appearance of biotite (Fig. S-3, Tables S-6, S-10), which dominates the Ti budget at low melt fraction (Fig. S-3, Tables S-6, S-10). The lower modal proportion of amphibole and earlier appearance of ilmenite in the fractional crystallisation model results in ilmenite being the dominant Ti-bearing phase (Fig. S-3, Table S-6, S-10). Clinopyroxene also possess a greater share of the Ti budget in comparison to the equilibrium models due to its higher modal abundance (Fig. S-3, Tables S-6, S-10).

4. Trace Element Modelling

For equilibrium partial melting and crystallisation models the trace element and Ti concentrations of the melt were calculated using the Equation S-1 (Shaw, 1970):

$$C_L = {}^{C_o}/_{D + F(1 - D)} \qquad \text{Eq. S-1}$$

where the trace-element composition of the liquid (C_L) depends on the composition of the source (C_0), the degree of partial melting (F), and the bulk distribution coefficient (D), itself a function of individual mineral partition coefficients

and mineral-melt proportions. The degree of melting, the residual mineral assemblage, and the associated mineral abundances are all controlled by the intensive and extensive chemical parameters (bulk composition, pressure, temperature, fluid pressure, oxygen fugacity etc.). Hence, this equation can be seen as relating C_L with (1) the nature of the mafic protolith and (2) the thermodynamic conditions of crustal evolution. This concept applies to melting and to crystallisation in the same way.

In fractional crystallisation scenarios a Rayleigh fractionation approach was used (Eq. S-2):

$$C_L = C_o D^{(1-F)} \qquad \text{Eq. S-2}$$

Trace element modelling always carries a certain degree of uncertainty, particularly in the case of TTG formation in which both amphibole and garnet are major residual phases (Foley, 2008; Qian and Hermann, 2013). The magnitude of D values in the literature for these phases varies greatly as function of pressure, temperature and melt composition, which is further compounded by the scarcity of experimental data relevant for tonalitic melts (Barth *et al.*, 2002; Foley, 2008; Klein *et al.*, 1997, 2000; Qian and Hermann, 2013). An effort was made to select experimentally determined mineral melt partition coefficients for tonalitic melts from the available published data at relevant pressure/temperature conditions (Barth *et al.*, 2002; Bédard, 2006; Klein *et al.*, 1997; Qian and Hermann, 2013). All mineral-melt partition coefficients ($D_{\text{min-melt}}$) used for trace element modelling are provided in Table S-7.

5. Modelling of Ti Isotope Fractionation

Equilibrium fractionation

Equilibrium isotope fraction during partial melting and crystallisation is governed by the following mass balance Equation S-3:

$$R^* = \frac{C_{melt}F_{melt}R_{melt}\alpha_{melt}+C_{amp}F_{amp}R_{melt}\alpha_{amp}+C_{cpx}F_{cpx}R_{melt}\alpha_{cpx}+\cdots}{C} \qquad \text{Eq. S-3}$$

In which R is an isotope ratio, $^{49}Ti/^{47}Ti$ in this case (relative to $^{49}Ti/^{47}Ti = 0.749766$ for OL-Ti), with a * used to represent the bulk composition. C is the concentration of Ti in a phase, F is the proportion of a phase, and α is the isotope fractionation factor between a given phase, (*i*) and the melt as defined by Equation S-4:

$$\alpha_i = \frac{R_i}{R_{melt}} \qquad \text{Eq. S-4}$$

The isotope mass balance equation can be rewritten as follows (Eq. S-5):

$$R^* = \frac{R_{melt}\sum_i(C_iF_i\alpha_i)}{C^*} \qquad \text{Eq. S-5}$$

If using mineral-melt partition coefficients the distribution of Ti (X_{Ti-i}) for each phase present can be calculated using (Eq. S-6):

$$X_{Ti-i} = \frac{F_i * D_{i-melt}^{Ti}}{\sum_n (F*D)} \quad \text{Eq. S-6}$$

Finally, in instances where the bulk isotope composition is known, the isotope composition of the melt can be obtained using the Equation S-7:

$$R_{melt} = \frac{R^* C^*}{\sum_i (C_i F_i \alpha_i)} \quad \text{Eq. S-7}$$

This equation was used to calculate the Ti isotope composition of melts produced during equilibrium melting and crystallisation. The isotope composition is reported relative to the Origins Lab Ti standard (Eq. S-8):

$$\delta^{49/47}Ti_{melt} = \left[\frac{R_{melt}}{R_{OL-Ti}}\right] - 1 \quad \text{Eq. S-8}$$

Rayleigh fractionation

Ti isotope fractionation during tonalite fractional crystallisation was obtained using a Rayleigh fractionation law. The Ti isotope composition of fractionated melts was obtained using the following Equation S-9:

$$R_{melt} = R_o f^{\alpha-1} \quad \text{Eq. S-9}$$

where, R is the $^{49}Ti/^{47}Ti$ isotope ratio, R^o is the initial isotope ratio, f is the fraction of Ti remaining in the melt, and α is the bulk solid-melt isotope fractionation factor between the remaining melt and the crystallizing mineral assemblage, where the mineral-melt fractionation factors are weighted by their Ti concentration at each stage of the model.
All Ti mineral melt fractionation factors are reported in Table S-8. The references for each of the main Ti-bearing phases are outlined below:

Fe-Ti oxides (rutile, ilmenite, magnetite) - Hoare *et al.* (2022); Rzehak *et al.* (2022)
Amphibole, biotite and sphene - Mandl (2019)
Clinopyroxene - Rzehak *et al.* (2022)
Orthopyroxene - Rzehak *et al.* (2021)
Garnet - Wang *et al.* (2020)

The phase proportions and Ti content of each phase are provided by the thermodynamic phase equilibria modelling for partial melting of metabasalts and tonalite crystallisation. In the case of partial melting models, the revised value of the bulk silicate Earth of +0.05 ± 0.01 ‰ from the recent study of Deng *et al.* (2023) was used as the initial bulk Ti isotope composition, which is indistinguishable from the weighted mean of the Isua metabasalts presented in this study ($\delta^{49/47}Ti$ = +0.052 ± 0.006 ‰; 95% c.i; n = 11). For tonalite crystallisation, the Ti isotope composition of JEH 10-38 was used (Table S-5). Whereas $\delta^{49/47}Ti$ composition of tonalite sample G97/31 was estimated via an exponential function of SiO_2 vs $\delta^{49/47}Ti$ using published data for Archean amphibolites and TTGs (n=48). The exponential function $\delta^{49/47}Ti = 2.3*10^{-}$

$^{4} * e^{1.04*10-1}$ (R^2 = 0.85) yielded a value of +0.23 ‰ for an SiO_2 content of 66.79 wt. % (Tables S-4, S-5, and S-11). This value is comparable to other TTG samples of similar SiO_2 contents (*e.g.* G91/61; Zhang *et al.*, 2023, Table S-11).

Supplementary Tables

Tables S-2 to S-11 are available for download (.xls) from the online version of this article at https://doi.org/10.7185/geochemlet.2342.

Table S-1 see page SI-2

Table S-2 see page SI-4

Table S-3 see pages SI-4 and SI-5

Table S-4 Whole rock geochemistry and Ti isotope compositions of Isua supracrustal belt metabasalts measured in this study.

Table S-5 Whole rock geochemistry and Ti isotope compositions of Itsaq Gneiss Complex samples measured in this study.

Table S-6 Results and output of Theriak/Domino phase equilibria modelling.

Table S-7 Mineral-melt partition coefficients and source compositions used for trace element modelling during partial melting and crystallisation.

Table S-8 Mineral-melt titanium isotope fractionation factors used for modelling of Ti isotope fractionation during partial melting and crystallisation.

Table S-9 Results of trace element and Ti isotope modelling for metabasalt partial melting.

Table S-10 Results of trace element and Ti isotope modelling for tonalite differentiation.

Table S-11 Compilation of literature whole rock geochemical data used in this study.

Supplementary Information References

Aarons, S.M., Reimink, J.R., Greber, N.D., Heard, A.W., Zhang, Z., Dauphas, N. (2020) Titanium isotopes constrain a magmatic transition at the Hadean-Archean boundary in the Acasta Gneiss Complex. *Science Advances* 6, eabc9959. https://doi.org/10.1126/sciadv.abc9959

Barling, J., Goldstein, S.L., Nicholls, I.A. (1994) Geochemistry of Heard Island (southern Indian Ocean): Characterization of an enriched mantle component and implications for enrichment of the sub-Indian Ocean mantle. *Journal of Petrology* 35,1017–1053. https://doi.org/10.1093/petrology/35.4.1017

Barth, M.G., Foley, S.F., Horn, I. (2002) Partial melting in Archean subduction zones: constraints from experimentally determined trace element partition coefficients between eclogitic minerals and tonalitic melts under upper mantle conditions. *Precambrian Research* 113, 323–340. https://doi.org/10.1016/S0301-9268(01)00216-9

Bédard, J.H. (2006) A catalytic delamination-driven model for coupled genesis of Archaean crust and sub-continental lithospheric mantle. *Geochimica et Cosmochimica Acta* 70, 1188–1214. https://doi.org/10.1016/j.gca.2005.11.008

de Capitani, C., Brown, T.H. (1987) The computation of chemical equilibrium in complex systems containing non-ideal solutions. *Geochimica et Cosmochimica Acta* 51, 2639–2652. https://doi.org/10.1016/0016-7037(87)90145-1

de Capitani, C., Petrakakis, K. (2010) The computation of equilibrium assemblage diagrams with Theriak/Domino software. *American Mineralogist* 95, 1006–1016. https://doi.org/10.2138/am.2010.3354

Chamberlain, K.J., Barclay, J., Preece, K.J., Brown, R.J., Davidson, J.P. (2019) Lower crustal heterogeneity and fractional crystallization control evolution of small-volume magma batches at ocean island volcanoes (Ascension Island, South Atlantic). *Journal of Petrology* 60, 489-1522. https://doi.org/10.1093/petrology/egz037

Clague, D.A., Caress, D.W., Dreyer, B.M., Lundsten, L., Paduan, J.B., Portner, R.A., Spelz‐Madero, R., Bowles, J.A., Castillo, P.R., Guardado‐France, R., Le Saout, M. (2018) Geology of the Alarcon Rise, southern Gulf of California. *Geochemistry, Geophysics, Geosystems* 19, 807-837. https://doi.org/10.1002/2017GC007348

Dempsey, S. (2013) *Geochemistry of volcanic rocks from the Sunda Arc* (Doctoral dissertation, Durham University).

Deng, Z., Moynier, F., Sossi, P.A., Chaussidon, M. (2018) Bridging the depleted MORB mantle and the continental crust using titanium isotopes. *Geochemical Perspectives Letters* 9, 11-15. https://doi.org/10.7185/geochemlet.1831

Deng, Z., Chaussidon, M., Savage, P., Robert, F., Pik, R., Moynier, F. (2019) Titanium isotopes as a tracer for the plume or island arc affinity of felsic rocks. *Proceedings of the National Academy of Sciences*, 116, 1132–1135. https://doi.org/10.1073/pnas.1809164116

Deng, Z., Schiller, M., Jackson, M.G., Millet, M.A., Pan, L., Nikolajsen, K., Saji, N.S., Huang, D., Bizzarro, M. (2023) Earth's evolving geodynamic regime recorded by titanium isotopes. *Nature* 621, 100-104. https://doi.org/10.1038/s41586-023-06304-0

Foley, S. (2008) A trace element perspective on Archean crust formation and on the presence or absence of Archean subduction. In: Condie, K.C., Pease, V. *When did plate tectonics begin on planet Earth? Geological Society of America* 440, 31. https://doi.org/10.1130/2008.2440(02)

Gale, A., Dalton, C.A., Langmuir, C.H., Su, Y., Schilling, J. (2013) The mean composition of ocean ridge basalts. *Geochemistry, Geophysics, Geosystems* 14, 489–518. https://doi.org/10.1029/2012GC004334

Greber, N.D., Dauphas, N., Bekker, A., Ptáček, M.P., Bindeman, I.N., Hofmann, A. (2017) Titanium isotopic evidence for felsic crust and plate tectonics 3.5 billion years ago. *Science* 357, 1271-1274. https://doi.org/10.1126/science.aan8086

Greber, N.D., Pettke, T., Vilela, N., Lanari, P., Dauphas, N. (2021) Titanium isotopic compositions of bulk rocks and mineral separates from the Kos magmatic suite: Insights into fractional crystallization and magma mixing processes. *Chemical Geology* 578, 120303. https://doi.org/10.1016/j.chemgeo.2021.120303

Green, E., White, R., Diener, J., Powell, R., Holland, T., Palin, R. (2016) Activity–composition relations for the calculation of partial melting equilibria in metabasic rocks. *Journal of Metamorphic Geology* 34, 845–869. https://doi.org/10.1111/jmg.12211

He, X., Ma, J., Wei, G., Zhang, L., Wang, Z., Wang, Q. (2020) A new procedure for titanium separation in geological samples for 49 Ti/47 Ti ratio measurement by MC-ICP-MS. *Journal of Analytical Atomic Spectrometry* 35, 100–106. https://doi.org/10.1039/C9JA00316A

He, X., Ma, J., Wei, G., Wang, Z., Zhang, L., Zeng, T., Zhang, Z., (2022) Mass-dependent fractionation of titanium stable isotopes during intensive weathering of basalts. *Earth and Planetary Science Letters* 579, 117347. https://doi.org/10.1016/j.epsl.2021.117347

Hoare, L., Klaver, M., Saji, N.S., Gillies, J., Parkinson, I.J., Lissenberg, C.J., Millet, M.-A. (2020) Melt chemistry and redox conditions control titanium isotope fractionation during magmatic differentiation. *Geochimica et Cosmochimica Acta* 282, 38–54. https://doi.org/10.1016/j.gca.2020.05.015

Hoare, L., Klaver, M., Muir, D.D., Klemme, S., Barling, J., Parkinson, I.J., Lissenberg, C.J., Millet, M.-A. (2022) Empirical and experimental constraints on Fe-Ti oxide-melt titanium isotope fractionation factors. *Geochimica et Cosmochimica Acta* 326, 253–272. https://doi.org/10.1016/j.gca.2022.02.011

Hoffmann, J.E., Münker, C., Næraa, T., Rosing, M.T., Herwartz, D., Garbe-Schönberg, D., Svahnberg, H. (2011a) Mechanisms of Archean crust formation inferred from high-precision HFSE systematics in TTGs. *Geochimica et Cosmochimica Acta* 75, 4157–4178. https://doi.org/10.1016/j.gca.2011.04.027

Hoffmann, J.E., Münker, C., Polat, A., Rosing, M.T., Schulz, T. (2011b) The origin of decoupled Hf–Nd isotope compositions in Eoarchean rocks from southern West Greenland. *Geochimica et Cosmochimica Acta* 75, 6610–6628. https://doi.org/10.1016/j.gca.2011.08.018

Hoffmann, J.E., Nagel, T.J., Muenker, C., Naeraa, T., Rosing, M.T. (2014) Constraining the process of Eoarchean TTG formation in the Itsaq Gneiss Complex, southern West Greenland. *Earth and Planetary Science Letter*s 388, 374–386. https://doi.org/10.1016/j.epsl.2013.11.050

Holland, T., Powell, R. (2011) An improved and extended internally consistent thermodynamic dataset for phases of petrological interest, involving a new equation of state for solids. *Journal of metamorphic Geology* 29, 333–383. https://doi.org/10.1111/j.1525-1314.2010.00923.x

Holland, T.J., Green, E.C., Powell, R. (2018) Melting of peridotites through to granites: a simple thermodynamic model in the system KNCFMASHTOCr. *Journal of Petrology* 59, 881–900. https://doi.org/10.1093/petrology/egy048

Holland, T.J.B., Green, E.C.R., Powell, R. (2022) A thermodynamic model for feldspars in KAlSi3O8− NaAlSi3O8− CaAl2Si2O8 for mineral equilibrium calculations. *Journal of Metamorphic Geology* 40, 587–600. https://doi.org/10.1111/jmg.12639

Jenner, F.E., Bennett, V.C., Nutman, A.P., Friend, C.R.L., Norman, M.D., Yaxley, G. (2009) Evidence for subduction at 3.8 Ga: geochemistry of arc-like metabasalts from the southern edge of the Isua Supracrustal Belt. *Chemical Geology* 261, 83–98. https://doi.org/10.1016/j.chemgeo.2008.09.016

Johnson, T.E., Gardiner, N.J., Miljković, K., Spencer, C.J., Kirkland, C.L., Bland, P.A., Smithies, H. (2018) An impact melt origin for Earth's oldest known evolved rocks. *Nature Geoscience* 11, 795–799. https://doi.org/10.1038/s41561-018-0206-5

Jørgensen, T.R., Tinkham, D.K., Lesher, C.M. (2019) Low‐P and high‐T metamorphism of basalts: Insights from the Sudbury impact melt sheet aureole and thermodynamic modelling. *Journal of Metamorphic Geology* 37, 271–313. https://doi.org/10.1111/jmg.12460

Kent, A., Stolper, E., Francis, D., Woodhead, J., Frei, R., Eiler, J. (2004) Mantle heterogeneity during the formation of the North Atlantic igneous province: Constraints from trace element and Sr‐Nd‐Os‐O isotope systematics of Baffin Island picrites. *Geochemistry, Geophysics, Geosystems* 5. https://doi.org/10.1029/2004GC000743

Klaver, M., Carey, S., Nomikou, P., Smet, I., Godelitsas, A., Vroon, P. (2016) A distinct source and differentiation history for Kolumbo submarine volcano, Santorini volcanic field, Aegean arc. *Geochemistry, Geophysics, Geosystems*, 17, 3254-3273. https://doi.org/10.1002/2016GC006398

Klaver, M., MacLennan, S.A., Ibañez-Mejia, M., Tissot, F.L., Vroon, P.Z., Millet, M.A. (2021) Reliability of detrital marine sediments as proxy for continental crust composition: The effects of hydrodynamic sorting on Ti and Zr isotope systematics. *Geochimica et Cosmochimica Acta* 310, 221-239. https://doi.org/10.1016/j.gca.2021.05.030

Klein, M., Stosch, H.-G., Seck, H. (1997) Partitioning of high field-strength and rare-earth elements between amphibole and quartz-dioritic to tonalitic melts: an experimental study. *Chemical Geology*. 138, 257–271. https://doi.org/10.1016/S0009-2541(97)00019-3

Klein, M., Stosch, H.-G., Seck, H., Shimizu, N. (2000) Experimental partitioning of high field strength and rare earth elements between clinopyroxene and garnet in andesitic to tonalitic systems. *Geochimica et Cosmochimica Acta*. 64, 99–115. https://doi.org/10.1016/S0009-2541(97)00019-3

Kommescher, S., Fonseca, R.O.C., Kurzweil, F., Thiemens, M.M., Münker, C., Sprung, P. (2020) Unravelling lunar mantle source processes via the Ti isotope composition of lunar basalts. *Geochemical Perspectives Letters* 13, 13–18. https://doi.org/10.7185/geochemlet.2007

Li, J., Tang, S., Zhu, X., Ma, J., Zhao, X. (2022) Titanium Isotope Analysis of Igneous Reference Materials using a Double‐spike MC‐ICP‐MS Method. *Acta Geologica Sinica‐English Edition* 96, 517-524. https://doi.org/10.1111/1755-6724.14728

Mancini, A., Mattsson, H.B., Bachmann, O. (2015) Origin of the compositional diversity in the basalt-to-dacite series erupted along the Heiðarsporður ridge, NE Iceland. *Journal of Volcanology and Geothermal Research*, 301, 116-127. https://doi.org/10.1016/j.jvolgeores.2015.05.010

Mandl, M.B. (2019) Titanium isotope fractionation on the Earth and moon: constraints on magmatic processes and moon formation. Doctoral dissertation, ETH Zurich.

Millet, M.-A., Dauphas, N., Greber, N.D., Burton, K.W., Dale, C.W., Debret, B., Macpherson, C.G., Nowell, G.M., Williams, H.M. (2016) Titanium stable isotope investigation of magmatic processes on the Earth and Moon. *Earth and Planetary Science Letters*. 449, 197–205. https://doi.org/10.1016/j.epsl.2016.05.039

Millet, M.A., Dauphas, N. (2014) Ultra-precise titanium stable isotope measurements by double-spike high resolution MC-ICP-MS. *Journal of Analytical Atomic Spectrometry*, 29, 1444–1458. https://doi.org/10.1039/C4JA00096J

Naeraa, T., Scherstén, A., Rosing, M.T., Kemp, A.I.S., Hoffmann, J.E., Kokfelt, T.F., Whitehouse, M.J. (2012) Hafnium isotope evidence for a transition in the dynamics of continental growth 3.2 Gyr ago. *Nature* 485, 627-630. https://doi.org/10.1038/nature11140

Nagel, T.J., Hoffmann, J.E., Münker, C. (2012) Generation of Eoarchean tonalite-trondhjemite-granodiorite series from thickened mafic arc crust. *Geology* 40, 375–378. https://doi.org/10.1130/G32729.1

Nash, W.P., Crecraft, H.R. (1985) Partition coefficients for trace elements in silicic magmas. *Geochimica et Cosmochimica Acta* 49, 2309-2322. https://doi.org/10.1016/0016-7037(85)90231-5

Nutman, A.P., Bennett, V.C., Friend, C.R., Norman, M.D. (1999) Meta-igneous (non-gneissic) tonalites and quartz-diorites from an extensive ca. 3800 Ma terrain south of the Isua supracrustal belt, southern West Greenland: constraints on early crust formation. *Contributions to Mineralogy and Petrology* 137, 364–388. https://doi.org/10.1007/s004100050556

Polat, A., Hofmann, A. (2003) Alteration and geochemical patterns in the 3.7–3.8 Ga Isua greenstone belt, West Greenland. *Precambrian Research* 126, 197–218. https://doi.org/10.1016/S0301-9268(03)00095-0

Qian, Q., Hermann, J. (2013) Partial melting of lower crust at 10–15 kbar: constraints on adakite and TTG formation. *Contributions to Mineralogy and Petrology* 165, 1195–1224. https://doi.org/10.1007/s00410-013-0854-9

Rzehak, L.J.A., Kommescher, S., Kurzweil, F., Sprung, P., Leitzke, F.P., Fonseca, R.O.C. (2021) The redox dependence of titanium isotope fractionation in synthetic Ti-rich lunar melts. *Contributions to Mineralogy and Petrology* 176, 1–16. https://doi.org/10.1007/s00410-020-01769-y

Rzehak, L.J., Kommescher, S., Hoare, L., Kurzweil, F., Sprung, P., Leitzke, F.P., Fonseca, R.O. (2022) Redox-dependent Ti stable isotope fractionation on the Moon: implications for current lunar magma ocean models. *Contributions to Mineralogy and Petrology* 177, 81. https://doi.org/10.1007/s00410-022-01947-0

Savage, P.S., Georg, R.B., Williams, H.M., Burton, K.W., Halliday, A.N. (2011) Silicon isotope fractionation during magmatic differentiation. *Geochimica et Cosmochimica Acta* 75, 6124-6139. https://doi.org/10.1016/j.gca.2011.07.043

Shaw, D.M. (1970) Trace element fractionation during anatexis. *Geochimica et Cosmochimica Acta*. 34, 237–243. https://doi.org/10.1016/0016-7037(70)90009-8

Storck, J.-C., Greber, N.D., Duarte, J.F.V., Lanari, P., Tiepolo, M., Pettke, T. (2023) Molybdenum and titanium isotopic signatures of arc-derived cumulates. *Chemical Geology* 617, 121260. https://doi.org/10.1016/j.chemgeo.2022.121260

Szymanowski, D., Ellis, B.S., Wotzlaw, J.F., Bachmann, O. (2019) Maturation and rejuvenation of a silicic magma reservoir: High-resolution chronology of the Kneeling Nun Tuff. *Earth and Planetary Science Letters* 510, 103-115. https://doi.org/10.1016/j.epsl.2019.01.007

Timm, C., Graham, I.J., de Ronde, C.E., Leybourne, M.I., Woodhead, J. (2011) Geochemical evolution of Monowai volcanic center: New insights into the northern Kermadec arc subduction system, SW Pacific. *Geochemistry, Geophysics, Geosystems* 12. https://doi.org/10.1029/2011GC003654

Wang, W., Huang, S., Huang, F., Zhao, X., Wu, Z. (2020) Equilibrium inter-mineral titanium isotope fractionation: Implication for high-temperature titanium isotope geochemistry. *Geochimica et Cosmochimica Acta* 269, 540–553. https://doi.org/10.1016/j.gca.2019.11.008

Wanke, M., Karakas, O., Bachmann, O. (2019) The genesis of arc dacites: the case of Mount St. Helens, WA. *Contributions to Mineralogy and Petrology* 174, 1–14. https://doi.org/10.1007/s00410-018-1542-6

White, R., Powell, R., Holland, T., Johnson, T., Green, E. (2014) New mineral activity–composition relations for thermodynamic calculations in metapelitic systems. *Journal of Metamorphic Geology* 32, 261–286. https://doi.org/10.1111/jmg.12071

Williams, N.H. (2015) Titanium isotope cosmochemistry. Doctoral dissertation, University of Manchester.

Williams, N.H., Fehr, M.A., Parkinson, I.J., Mandl, M.B., Schönbächler, M. (2021) Titanium isotope fractionation in solar system materials. *Chemical Geology* 568, 120009. https://doi.org/10.1016/j.chemgeo.2020.120009

Xiong, X.L. (2006) Trace element evidence for growth of early continental crust by melting of rutile-bearing hydrous eclogite. *Geology* 34, 945-948. https://doi.org/10.1130/G22711A.1

Zhang, J., Dauphas, N., Davis, A.M., Pourmand, A. (2011) A new method for MC-ICPMS measurement of titanium isotopic composition: Identification of correlated isotope anomalies in meteorites. *Journal of Analytical Atomic Spectrometry* 26, 2197–2205. https://doi.org/10.1039/c1ja10181a

Zhang, Z.J., Dauphas, N., Johnson, A.C., Aarons, S.M., Bennett, V.C., Nutman, A.P., MacLennan, S., Schoene, B. (2023) Titanium and iron isotopic records of granitoid crust production in diverse Archean cratons. *Earth and Planetary Science Letters* 620, 118342. https://doi.org/10.1016/j.epsl.2023.118342